Current Biology *16*, 702–709, April 4, 2006 ©2006 Elsevier Ltd All rights reserved DOI 10.1016/j.cub.2006.02.063

Report

The Tumor Suppressors Merlin and Expanded Function Cooperatively to Modulate Receptor Endocytosis and Signaling

Sushmita Maitra,[1] Rima M. Kulikauskas,[2] Heather Gavilan,[2] and Richard G. Fehon[1,*]
[1] Department of Molecular Genetics and Cell Biology
University of Chicago
Chicago, Illinois 60637
[2] DCMB Group
Department of Biology
Duke University
Box 91000
Durham, North Carolina 27708

Summary

The precise coordination of signals that control proliferation is a key feature of growth regulation in developing tissues [1]. While much has been learned about the basic components of signal transduction pathways, less is known about how receptor localization, compartmentalization, and trafficking affect signaling in developing tissues. Here we examine the mechanism by which the *Drosophila Neurofibromatosis 2* (*NF2*) tumor suppressor ortholog *Merlin* (*Mer*) and the related tumor suppressor *expanded* (*ex*) regulate proliferation and differentiation in imaginal epithelia. Merlin and Expanded are members of the FERM (Four-point one, Ezrin, Radixin, Moesin) domain superfamily, which consists of membrane-associated cytoplasmic proteins that interact with transmembrane proteins and may function as adapters that link to protein complexes and/or the cytoskeleton [2]. We demonstrate that Merlin and Expanded function to regulate the steady-state levels of signaling and adhesion receptors and that loss of these proteins can cause hyperactivation of associated signaling pathways. In addition, pulse-chase labeling of Notch in living tissues indicates that receptor levels are upregulated at the plasma membrane in *Mer; ex* double mutant cells due to a defect in receptor clearance from the cell surface. We propose that these proteins control proliferation by regulating the abundance, localization, and turnover of cell-surface receptors and that misregulation of these processes may be a key component of tumorigenesis.

Results and Discussion

Merlin's tumor suppressor function is conserved from humans to flies [3], but the cellular basis for this function remains unclear. Genetic studies in *Drosophila* suggest that *Mer* regulates signaling pathways that control proliferation [4], and cell biological experiments indicate that Merlin may play a role in endocytic processes [3, 5]. In addition, Merlin physically interacts with Expanded, a distantly related member of the FERM superfamily, and these proteins colocalize in the apical junctional region of epithelial cells. Furthermore, genetic studies have shown that while mutations of each gene produce modest overproliferation phenotypes in the eye and wing [3, 6, 7] (see Figures S1 and S2 in the Supplemental Data available with this article online), double mutant *Mer; ex* cells display severe overgrowth and differentiation defects that are not seen in either mutation alone. Thus, *Mer* and *ex* are partially redundant in regulating proliferation and differentiation [7].

Given these observations, we reasoned that the difficulty in identifying precise cellular functions for Merlin might stem from its redundancy with Expanded and that this difficulty could be overcome by examining tissues from double mutant animals and double mutant cell clones generated by somatic recombination. Overproliferation of *Mer; ex* wing imaginal discs is more extreme than that observed with either mutation alone (Figure S2). Surprisingly, however, Mer^{4}; ex^{697} eye-antennal imaginal discs have severely reduced eye primordia with a substantial reduction in or total absence of photoreceptors, although the antennal portion is normal or slightly larger than normal (Figures 1A–1D) and occasionally is duplicated (data not shown). Apoptosis does not appear to be enhanced in double mutant eye-antennal discs (data not shown), suggesting that loss of the eye primordium is not due to cell death. Thus, loss of *Mer* and *ex* function has a tissue-specific defect in the developing eye that is very different from its effects on proliferation in the wing imaginal disc.

Why does the combined loss of two tumor suppressors cause reduction rather than hypertrophy of eye tissue? Previous studies have shown that initiation of the morphogenetic furrow, which organizes development of the eye, is regulated by a complex network of signals at the posterior and lateral margins of the eye-antennal disc [8, 9]. Mutations that affect these signals not only block furrow initiation, but also may significantly reduce the size of the eye field and disrupt photoreceptor differentiation. For example, ectopic Wingless expression either at the posterior and lateral margins [10] or throughout the eye primordium [11] results in dramatic losses of eye tissue that closely resemble the *Mer; ex* phenotype just described. Similar effects are seen from reduction in Decapentaplegic (DPP) or Hedgehog signaling in the same cells [12, 13].

If Merlin and Expanded affect initiation of the morphogenetic furrow rather than differentiation of photoreceptors, then *Mer; ex* double mutant somatic clones should block ommatidial development only when present at the posterior or lateral margins of the eye field. Indeed, we observed that *Mer; ex* clones could differentiate photoreceptors, but only when located in the middle of the eye field (Figures 1E and 1F). In contrast, clones in contact with the posterior or lateral margin of the eye fail to produce photoreceptors. We infer from these observations that one or more of the signaling pathways that control

*Correspondence: rfehon@uchicago.edu

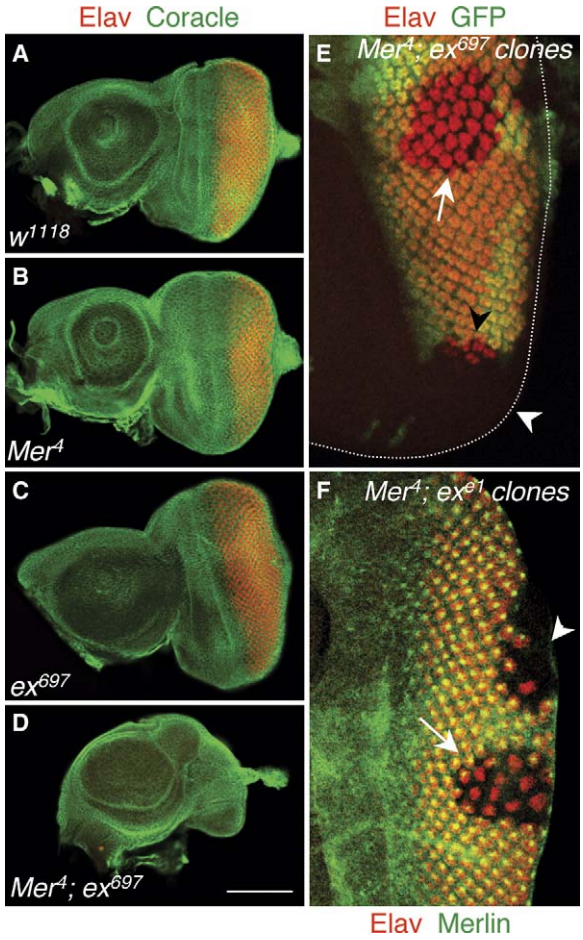

Figure 1. Simultaneous Loss of Merlin and Expanded Functions Result in Reduction of the Eye Field and a Lack of Photoreceptor Differentiation

(A–D) Eye-antennal disc complexes stained with anti-Coracle (membrane marker, green) and Elav (photoreceptors, red). Posterior is to the right in these and subsequent images of larval eye imaginal discs. In the control eye-antennal complex (A), anti-Elav staining reveals the regular array of differentiating photoreceptors. Loss of *Mer* (B) or *ex* (C) alone does not affect formation of photoreceptors. In contrast, photoreceptor development and overall eye field size are severely reduced in double mutant discs (D).

(E and F) Somatic mosaic analysis of *Mer; ex* cells in the eye. Mutant cell clones are negatively marked by absence of GFP ([E], green) or Merlin ([F], green). Clones of double mutant cells (E and F) completely contained within the eye field differentiate photoreceptors (white arrows; note there is a thin strip of wild-type cells at the posterior margin of the clone in [F]), but clones that encompass the lateral or posterior margin have significantly reduced numbers of photoreceptors (white arrowheads). Dotted line indicates the boundary of the eye epithelium in (E). The clone in (E) that touches the lateral boundary has a few photoreceptors (black arrowhead) in the mutant tissue. These photoreceptors presumably developed by passage of the morphogenetic furrow that had initiated within the wild-type tissue at the posterior margin.

Scale bar equals 100 μm (A–D) and 30 μm (E and F).

initiation of the morphogenetic furrow are likely disrupted in *Mer; ex* double mutant cells.

Signaling and Adhesion Receptors Are Upregulated in *Mer; ex* Double Mutant Cells

Given that Merlin is associated with the plasma membrane and may function in endocytic processes [5], we decided to ask if Merlin and Expanded play a role in regulating localization and/or abundance of transmembrane receptors that function in eye development. For these studies, we examined *Mer; ex* somatic mosaic cell clones to allow side-by-side comparisons of wild-type and mutant cells in the wing and eye imaginal discs. Immunofluorescence staining with specific antibodies then allowed us to compare the steady-state levels of receptors between adjacent wild-type and mutant cells. Intriguingly, Notch, the EGF receptor, Patched, and Smoothened all displayed increased antibody staining in double mutant cells relative to their wild-type neighbors (Figures 2A–2J). Notch, which is primarily localized to the apical junctional domain in wild-type cells, showed not only increased junctional staining in mutant cells, but also more diffuse staining (Figures 3A′ and 3B′). Similarly, preparations with anti-EGFR display more abundant membrane-associated and cytoplasmic staining in mutant than in wild-type cells (Figures 2A and 2B; data not shown). Patched staining, which is less obviously junctional than Notch or EGFR, appeared more punctate in *Mer; ex* cells (Figures 2E–2H). Thus, simultaneous loss of Merlin and Expanded results in increased abundance of receptors for multiple signaling pathways, though the precise localization defect seems to be specific to each receptor. We also examined two adhesion-related receptors, E-cadherin and Fat, a cadherin superfamily member, and found that both are similarly upregulated in *Mer; ex* cells (Figures 2K–2N). However, Coracle, a membrane-associated cytoplasmic protein, is not affected (Figures 2O and 2P). In addition, the localization of markers for apical-basal polarity, including DLG, PATJ, and aPKC, was unaffected in the double mutant cells, indicating that epithelial polarity is not disrupted (data not shown). In contrast to the double mutant cells, clones lacking just *Merlin* show no apparent difference in receptor localization or abundance, and ex^{e1} cells display only a slight increase in staining (Figure S3; data not shown). Taken together, these results indicate that Merlin and Expanded are required to reduce the steady-state abundance of a variety of signaling and adhesion receptors in developing epithelia.

Mer; ex Mutant Cells Display Membrane Trafficking Defects

To determine the cause for increased receptor abundance, we first tested the possibility that their expression is transcriptionally upregulated in mutant cells. We used quantitative PCR to determine the levels of the EGFR transcript in imaginal discs from Mer^4; ex^{697} double mutant larvae and found that it is downregulated ~4-fold (2.1 ± 0.3 cycle difference). This observation is consistent with previous observations that EGFR pathway activation feeds back negatively on its expression at the level of transcription [14], suggesting that EGFR signaling is upregulated in *Mer; ex* mutant cells. Similar experiments looking at Notch transcript levels showed no effect on Notch expression (data not shown). Thus, it does not appear that the observed effects in *Mer; ex* cells are due to misregulation at the transcriptional level.

These results suggest an alternative possibility—that membrane trafficking is affected in *Mer; ex* double mutant cells. To address this hypothesis, we used antibodies against the extracellular domain of Notch

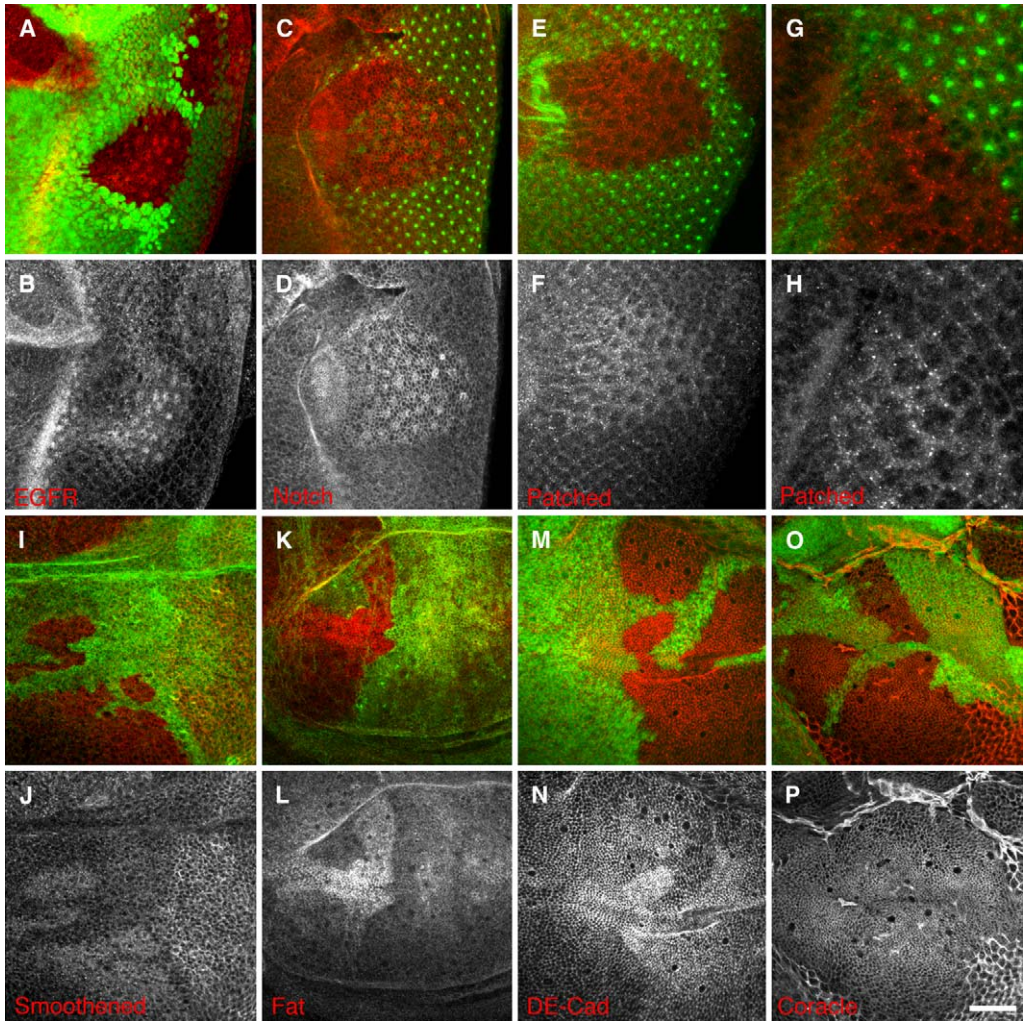

Figure 2. Steady-State Levels of Transmembrane Receptors Are Elevated in *Mer*; *ex* Double Mutant Clones

Mer^4; ex^{e1} clones in eye (A–H) and wing (I–P) imaginal discs. Mutant tissue is marked by the absence of Merlin staining ([C–L], green) or GFP ([A, B, M–P], green). Proteins of interest are shown in red in the merged panels (A, C, E, G, I, K, M, O) and separately in the corresponding lower panels (B, D, F, H, J, L, N, P). Receptor proteins, EGFR (A and B), Notch (C and D), Patched (E–H), Smoothened (I and J), and membrane adhesion proteins Fat (K and L), and DE cadherin (M and N), show increased staining in the double mutant tissue. Coracle (O and P), which is membrane associated, is not altered in mutant cells. Higher magnification views of Patched (G and H) shows that the staining is both punctate and cytoplasmic. Panels are maximum projections of z series. Scale bar equals 60 μm (A and B), 25 μm (C–F and I–P), and 10 μm (G and H).

(anti-ECN) to label protein on the surface of living cells in imaginal discs bearing somatic mosaic clones. Side-by-side comparisons of wild-type and *Mer; ex* mutant cells show increased cell-surface Notch labeling, consistent with what we observed with fixed tissue and indicating that there are increased levels of receptor at the plasma membrane in mutant cells (Figures 3C, 3D, 3C′, 3D′, 3O, and 3P). In addition, in double mutant cells, the junctional band of Notch staining is broader (Figures 3C, 3D, 3C′, and 3D′), indicating that Notch localization to the junctional region also may be affected. Similar differences in junctional staining were observed with the same antibody on fixed and permeabilized tissues, indicating that surface labeling of live cells does not affect Notch localization (Figures 3A–3D and 3A′–3D′).

To ask if the increased abundance is due to a defect in turnover, we used a pulse-chase approach to label Notch receptor at the plasma membrane and then followed its removal from the cell surface. To restrict our analysis to Notch that remains at the cell surface, tissues were fixed but not permeabilized at the end of the chase period. We observed a progressive loss of Notch staining at the cell surface during the chase period that appeared more rapid in wild-type than in mutant cells (Figures 3C–3J), suggesting a defect in trafficking off the plasma membrane. We used quantitative fluorescence analysis to determine the relative quantities of Notch on wild-type and mutant cells at the various chase time points. The results indicate that the ratio of cell-surface Notch fluorescence in mutant versus wild-type cells increases significantly between 0 and 10, 30, or 60 min postlabeling (Table 1). Therefore, Notch protein is cleared more rapidly from the surface of wild-type than mutant cells.

Three lines of evidence indicate that this procedure has no effect on receptor behavior or activation state. First, control experiments with the mAb323 antibody to *E(spl)* bHLH proteins [15] indicate that treatment with

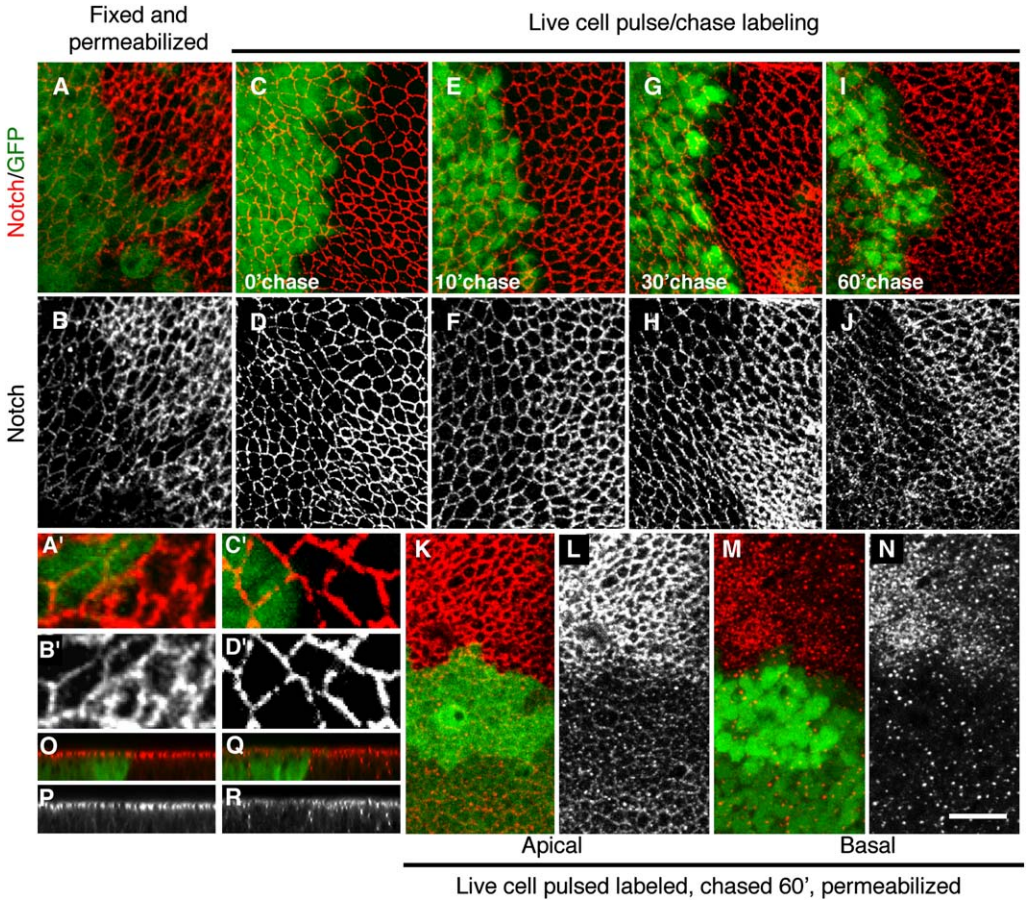

Figure 3. Trafficking of Notch from the Plasma Membrane Is Slower in *Mer; ex* Cells

Antibody labeling of the Notch extracellular domain in fixed and permeabilized (A, B, A′, B′) or live (C–R, C′, D′) wing imaginal discs that carry *Mer*^{4}*; ex*^{e1} double mutant clones. (A)–(N) display projections through multiple optical sections. (A′)–(D′) show high-magnification projections at the border of clones shown in (A)–(D). Clones are marked by absence of GFP (green). Anti-Notch staining is shown in red in the merged panels (A, A′, C, C′, E, G, I, K, M, O, and Q) and singly in the remaining panels (B, B′, D, D′, F, H, J, L, N, P, and R). (A, B, A′, B′) Fixed, permeabilized wing disc stained with an antibody that recognizes an extracellular epitope of Notch (anti-ECN). Compared to wild-type cells, Notch staining is elevated and more diffuse in double mutant cells. (C–R, C′, D′) Live wing imaginal discs pulse labeled with anti-ECN, rinsed, and either fixed immediately (C, D, C′, D′, O, P) or chased (E–N, Q–R) to follow Notch trafficking. In (C)–(J), the secondary antibody was incubated in the absence of detergent so that only anti-ECN that remained on the cell surface was labeled. In (K)–(R), detergent was added during secondary antibody incubation to reveal intracellular Notch protein that had trafficked from the plasma membrane. The absence of internal Notch staining (from synthesis and internalization) results in a much sharper image in nonpermeabilized than in permeabilized tissue (compare [D] to [B], [D′] to [B′]). 0 min chase (C, D, C′, D′, O, P): both nonpermeabilized tissue (C, D, C′, D′) and permeabilized tissue (O and P) show distinct junctional staining and only a slight increase in Notch staining in double mutant cells. At this time point, there is little or no detectable cytoplasmic staining (P). 10 min (E and F) and 30 min (G and H) chase: Differences in nonpermeabilized anti-ECN staining between wild-type and mutant cells are quite apparent at both time points. There is elevated staining in mutant cells relative to wild-type cells, and it appears less clearly associated with the junctional region. 60 min chase (I–N, Q–R): apical region of cells in both nonpermeabilized (I and J) and permeabilized (K and L) tissue show that junctional anti-ECN staining is substantially reduced in wild-type cells but still obvious in mutant cells. More basally in permeabilized tissues (M and N), punctate staining is seen in both wild-type and mutant cells, with the latter showing larger number of punctae and diffuse cytoplasmic stain. Optical cross-sections (Q and R) confirm the presence of apical junctional and subapical punctate staining in both cell types. Scale bar equals 10 μm (A–N), 15 μm (O–R), 2 μm (A′–D′).

anti-ECN does not affect Notch signaling (data not shown). Second, this procedure had no detectable effect on Notch localization, indicating that the antibody treatment does not induce receptor internalization (Figure S4). Third, monovalent Fab fragments of the anti-Notch antibody behaved identically in these experiments to the intact IgG monoclonal (Figure S4), indicating that the intact IgGs did not induce artifacts through static interference or receptor cross-linking.

It is worth noting that current models for Notch receptor activation require cleavage and release of its extracellular domain in response to ligand binding [16]. Because we used an antibody that recognizes this domain, it follows that our studies examined only ligand-independent trafficking of the receptor. In support of this inference, the pattern of Notch internalization in pulse-chase experiments was unaffected in *Delta*$^{-}$ clones (data not shown). These observations suggest that Merlin and Expanded function in steady-state, ligand-independent clearance of receptors from the plasma membrane, rather than internalization and degradation that occurs in response to ligand binding.

Table 1. Quantitation of Notch Clearance from the Plasma Membrane

	Chase Period			
	0 min	10 min	30 min	60 min
Ratio (mut/wt)	2.33	2.93	3.06	2.92
SE	±0.13	±0.27	±0.32	±0.23
n	18	17	17	16
p value		0.03	0.02	0.02

The ratio of total anti-ECN fluorescence was determined in mutant cells relative to wild-type cells at the indicated time points as described in the Experimental Procedures. Standard error (SE), the number of mutant clones scored (n), and p values relative to the 0 min time point (by means of a single-tailed t test) are indicated below the ratios.

We wondered if in addition to a defect in clearance from the plasma membrane, *Mer; ex* cells might also be defective in degradation of Notch receptors once they have been internalized. Imaginal epithelia pulse chased with anti-ECN display cytoplasmic punctae of Notch staining that are visible only in detergent-permeabilized preparations, indicating that they represent endocytic compartments. These punctae appear more numerous in mutant cells at a later time point (Figures 3K–3N, 3Q–3R). This result indicates that receptors can be internalized from the surface of mutant cells and raises the possibility of an additional defect in degradation of receptors after internalization. Further studies will be required to clarify the nature of this defect.

Merlin and Expanded Can Function to Limit Signaling Pathway Output

Increased receptor abundance may be expected to result in increased signaling output, if receptor quantity is a limiting factor. In addition, even if overall receptor quantity is not limiting, alterations in subcellular localization or the dynamics of receptor trafficking may have dramatic effects on receptor function. To ask if loss of Merlin and Expanded result in increased output from signaling pathways that regulate eye development and cell proliferation, we used markers specific for downstream activation of the EGFR, Wingless, and Notch signaling pathways (Figure 4). First, we stained double mutant clones with an antibody that recognizes the phosphorylated, activated form of MAP kinase (anti-dpERK), a downstream effector of the EGFR pathway (Figures 4A–4C). In addition to the normal anti-dpERK pattern in the wing imaginal disc, we observed increased staining in *Mer; ex* clones relative to their wild-type neighbors, suggesting upregulation of EGFR pathway activity. Similarly, output from the Wingless pathway was monitored by looking at expression of Distalless, a target of Wingless signaling [17] and found to be dramatically higher in the double mutant wing clones (Figures 4D–4F). In contrast, similar experiments with the mAb323 antibody to *E(spl)* bHLH proteins, a marker for Notch pathway activity, did not show upregulation of Notch signaling (data not shown). This result is consistent with the observation that overexpression of Notch in a wild-type genetic background has little or no phenotype [18]. To examine this further, we analyzed a genetic context in which Notch receptor quantities are known to be limiting—in animals that are heterozygous for a null *Notch* mutation. Such animals display a dominant, haploinsufficient phenotype characterized by notching along the wing margin. To ask if reduction in Merlin and Expanded in this context can cause upregulation of Notch pathway output, we generated animals triply heterozygous for *Notch*, *Merlin*, and *expanded* and found that the characteristic *Notch* wing phenotype was strongly suppressed (Figures 4G–4I).

Taken together, these results are consistent with our observation that the steady-state level of multiple receptors is elevated in *Mer; ex* cells and indicate that, depending on the precise developmental or genetic context, loss of Merlin and Expanded can result in increased output from the corresponding signaling pathways. In *Mer; ex* eyes, upregulation of Wingless signaling may be a primary contributor to the observed defect in ommatidial development. Previous studies have shown that ectopic Wingless signaling produces remarkably similar eye phenotypes [10, 11, 19], and our preliminary data suggest that inhibiting Wingless signaling partially suppresses the *Mer; ex* eye phenotype (data not shown). In the wing, the dramatic overproliferation of *Mer; ex* cells may be the combined result of upregulation of several pathways, including EGFR and Wingless.

Our previous studies have shown that Merlin and Expanded are associated with the apical junctional region in imaginal epithelia and with endocytic vesicles in cultured cells [5, 7]. Results shown here indicate that loss of these proteins affects abundance, cell-surface localization, and endocytic trafficking of Notch, EGFR, and other signaling and adhesion receptors in epithelial cells. Recent studies of endocytic trafficking in receptor/ligand regulation [16, 20] suggest aspects of endocytosis that could relate to Merlin and Expanded function. For example, it is possible that Merlin and Expanded function at the plasma membrane to recruit or anchor transmembrane proteins at sites on the membrane from which they are endocytosed or in the sorting between recycling endosomes and lysosomal degradation by promoting receptor degradation. Both possibilities are consistent with our observations of increased receptor levels at the plasma membrane in *Mer; ex* mutant cells (Figures 2 and 3) and colocalization of Merlin and Expanded with Notch in punctate structures at the plasma membrane (Figure S5). In addition, we have observed a partial colocalization of Merlin and Expanded with Rab 11, a marker for recycling endosomes, and with EEA-1, which labels early endosomes (Figure S6). Intriguingly, a previous study has suggested that the closely related ERM protein Ezrin functions to promote recycling rather than degradation of the β2-adrenergic receptor via its interactions with filamentous actin [21]. Understanding the exact relationship of Merlin and Expanded to endocytosis and recycling of receptors, as well as their possible relationship to ERM proteins in this process, will require further analysis.

A recent study has proposed that Merlin and Expanded function upstream of Hippo in the Warts signaling pathway, which regulates proliferation [22]. As noted in their study, *Merlin* and *expanded* mutants display similar phenotypes to those seen in *hippo* mutants. However, there are significant phenotypic differences between *Mer; ex* and *hippo* mutations, most notable of

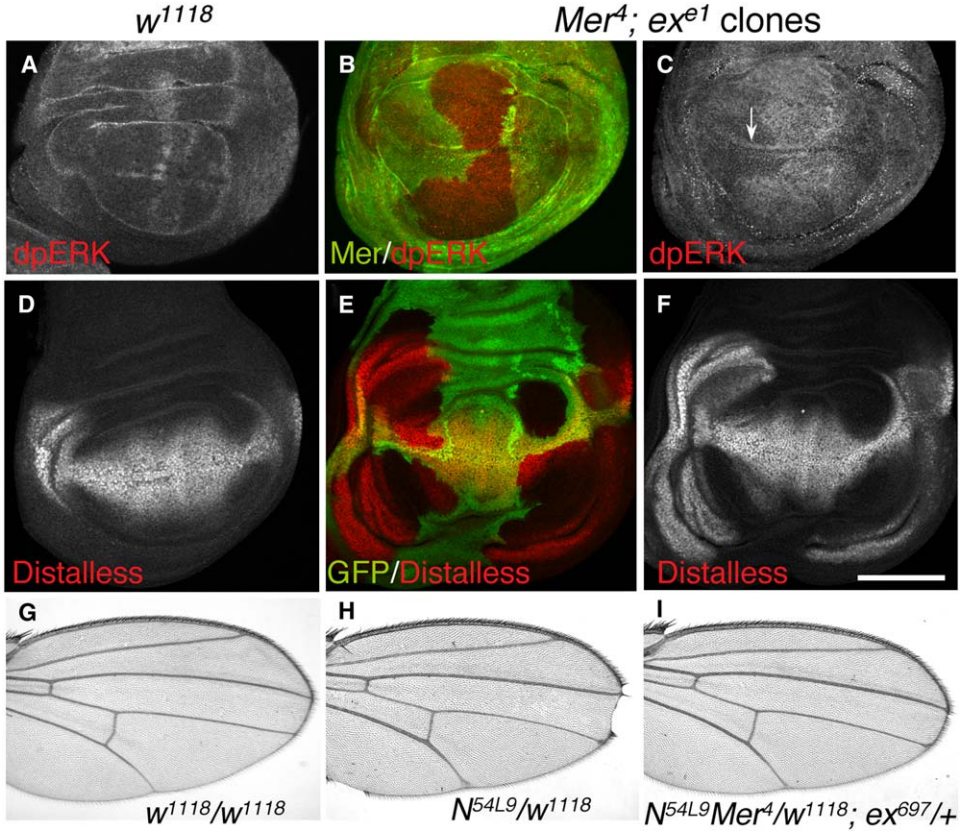

Figure 4. Signaling Pathway Outputs Are Affected by Loss of Merlin and Expanded

(A–C) Wing imaginal discs stained for dpERK, a marker for activation of the EGFR pathway ([A], w^{1118}, [B and C], Mer^{4}; ex^{e1} clones). Double mutant tissue is marked by the absence of green in (B) (anti-Merlin). In addition to the normal pattern of dpERK staining (the arrow indicates endogenous ERK activation at the dorsoventral boundary in [C]), there is increased staining within the clone of double mutant cells.

(D–F) Distalless expression in wing imaginal discs used as an indicator of wingless signaling output ([D], w^{1118}; [E and F], Mer^{4}; ex^{e1} clones). Note the increased anti-Distalless staining in mutant clones in the proximal regions (edges) of the wing blade, where Distalless is normally expressed.

(G–I) Wings from adult *Drosophila* females: (G) w^{1118}; (H) N^{54L9}/w^{1118}. Haploinsufficiency for the *Notch* locus results in notches at the wing margin. This phenotype is seen in essentially all flies of this genotype.

(I) N^{54L9} Mer^{4}/w^{1118}; ex^{697}/+. The Notch phenotype is strongly suppressed in this genotype.

Scale bar equals 100 μm (A–F).

which is that *hippo* mutations have not been reported to block induction of eye morphogenesis. In addition, there is no evidence to suggest that the Hippo pathway regulates output of the EGFR, Wingless, or Notch signaling pathways. Thus, the relationship of Merlin and Expanded to the Hippo pathway may be more complicated than the linear pathway proposed. One possibility is that Hippo activation is a downstream consequence of Merlin and Expanded's effects on output of multiple signaling pathways as we have shown here.

More than a decade after its molecular characterization, the precise cellular functions of Merlin in regulating cell proliferation remain unclear. Based on our studies, we propose that *Merlin*'s tumor suppressor phenotype results from defects in endocytic trafficking of signaling receptors and accompanying hyperactivation of associated signaling pathways. Recent studies highlight the importance of endocytosis in regulation of signaling pathways [16, 20]. Based on the results presented here, we suggest that proper regulation of membrane trafficking also may have important implications for understanding the cellular basis of tumor suppression in flies and mammals.

Experimental Procedures

Drosophila *Stocks and Genetics*

Stocks carrying *Merlin* null (Mer^{4}) and *expanded* hypomorphic (ex^{697}) mutations were used to build the following double mutant stock: *y w* Mer^{4} *FRT19A/FM7, P{ActGFP};* ex^{697}*/CyO, P{ActGFP}*. Controls stocks used were w^{1118} for the BrdU incorporation experiments and analysis of pupal eye structure and *y w FRT19A* for analysis of larval eye-antennal disc structure and quantitative PCR experiments. All stocks used to build recombinant chromosomes and for crosses to generate clones were obtained from the Bloomington *Drosophila* Stock Center except where noted.

Mer^{4}; ex^{e1} double mutant clones were obtained by crossing either *y w* Mer^{4}*FRT19A; P{Ubi-Mer*$^{+}$*}, P{Ubi-GFP*^{nls}*}, FRT40A/CyO, P{ActGFP}*, or *y w* Mer^{4}*FRT19A; P{Ubi-Mer*$^{+}$*} FRT40A/CyO, P{ActGFP}* females to *w/Y;* ex^{e1} *FRT40A/CyO, P{ActGFP}; MKRS, P{hsflp}/TM6, Tb, Hu* males. Mer^{4}; ex^{697} double mutant clones were obtained via a similar scheme. Single mutant clones for *Merlin* were obtained by crossing *y w* Mer^{4}*19AFRT; P{Ubi-Mer*$^{+}$*}, P{Ubi-GFP*^{nls}*}, FRT40A/CyO, P{ActGFP}* females to *w/Y; FRT40A;MKRS, P{hsflp}/TM6, Tb, Hu* males. ex^{e1} clones were obtained by crossing *w;* ex^{e1} *FRT40A/CyO, P{ActGFP}; MKRS, P{hsflp}/TM6, Tb, Hu* females to *y w/Y; P{Ubi-GFP}33, P{Ubi-GFP}38, FRT40A* males. In all the above crosses, clones were detected either by absence of GFP fluorescence or by anti-Merlin staining. For somatic mosaic analysis, uncrowded collections (5–10 hr) were made in vials, heat

shocked (1 hr at 37ºC, 1 hr at 25ºC, 1 hr at 37ºC) 33–48 hr after egg collection (AEL), and dissected at the wandering third instar stage.

To obtain single and double mutant animals, embryo collections were made on apple juice plates for 12 hr. Approximately 40 non-GFP (mutant) and 20 GFP (wild-type) larvae were transferred to food vials at 25ºC to allow the animals to grow under uncrowded conditions. Wandering third instar non-GFP male larvae were dissected for imaginal discs. For pupal eye dissections, white prepupae were collected and aged for 24 hr at 25ºC.

To study genetic interactions between *Merlin*, *expanded*, and *Notch*, females from N^{54L9}*/FM6* and *y w* N^{54L9} Mer^{4} *FRT19A/FM7, P{ActGFP};* ex^{697}*/CyO, P{ActGFP}* stocks were out-crossed to w^{1118} males and the F1 progeny scored for the wing notching phenotype.

Antibody Production

The anti-Expanded antibody was produced by immunizing guinea pigs with a fusion protein encompassing amino acids 145–947 fused to glutathione S transferase.

Immunofluorescence

Wandering third instar larvae or 24 hr pupae were dissected in Schneider's medium to obtain eye-antennal or wing imaginal discs. Tissues for anti-EGFR staining were dissected in serum-free Schneider's medium. Tissues were processed for immunofluorescence as described previously [23], with the following exceptions. For detection of dpERK, tissues were dissected in phosphate buffer, fixed in paraformaldehyde-lysine-phosphate buffer [24], and blocked in 10% normal goat serum with 0.1% Triton X-100 (K. Moses, personal communication). For BrdU incorporation, previously described methods [25] were used. Antibodies recognizing the following epitopes were used: BrdU (1:1,000, mouse, Zymed); Coracle (1:10,000, guinea pig [26]); DE cadherin (1:200, rat, provided by T. Uemura); Distalless (1:500, provided by I. Duncan); dpERK (1:100, mouse, Clone MAPK-YT, Sigma); EEA1 (1:1,000, from Abcam, Inc); EGFR (1:20,000, rabbit, provided by E. Bach); Elav (1:1,000, mouse, Developmental Studies Hybridoma Bank, DHSB); Expanded (1:5,000, guinea pig, this report); Fat (1:1,000, rat, provided by M. Simon); Merlin (1:10,000, guinea pig polyclonal [5]); Notch intracellular domain (1:10,000, mouse, clone C17.9C6 [27]); Notch extracellular domain (1:500, mouse, clone C458.2H, DHSB, also referred to as anti-ECN in this report); Patched (1:50, mouse, provided by I. Guerrero); Rab5 (1:250, provided by M. Gonzales-Gaitan); Rab11 (1:20,000, provided by D. Ready), and Smoothened (1:1,000, mouse, DHSB). To reduce nonspecific staining, blocking solution was supplemented with 5% milk for anti-EGFR, and the Expanded and Patched antibodies were preabsorbed against *Drosophila* larval tissue. Secondary antibodies (diluted 1:1,000) were from Jackson Immunoresearch Laboratories. Images were obtained and analyzed with either a Zeiss LSM 410 or LSM 510 confocal microscope and prepared with Adobe Photoshop 6.0.

Live Notch Labeling and Detection

Wing imaginal discs were dissected in Schneider's medium from wandering third instar larvae. The peripodial membrane was torn with a tungsten needle to promote antibody access to the apical membrane of the disc epithelium. Discs were washed once in cold Schneider's medium and pulse labeled with mouse anti-Notch C458.2H (a 1:2 mix of hybridoma culture supernatant in Schneider's medium) for 15 min on ice. After washing three times in cold Schneider's medium on ice, the discs were either fixed immediately or transferred to Schneider's medium at room temperature for 10, 30, or 60 min. Fixation was done in 4% paraformaldehyde (in PBS) at room temperature for 30 min. Tissues were blocked either in PBS with 0.1% Triton X and 1% goat serum (for the permeabilized set) or in PBS with 1% goat serum alone (for the nonpermeabilized set). Alexa Fluor 586 (Molecular Probes) coupled secondary antibody was used at 1:2000. Images were taken as described before.

For experiments with Fab fragments, ascites fluid containing mouse anti-Notch C458.2H (obtained from DHSB) was purified and cleaved with the Pierce Immunopure IgG_1 Fab preparation kit following manufacturer's instructions. Complete cleavage was confirmed by SDS-PAGE analysis.

Quantitative Measurements of Immunofluorescence Images

To compare relative fluorescence, Z-series sections were collected through imaginal discs containing somatic mosaic clones so that adjacent mutant and wild-type cells could be compared directly in a pairwise fashion. Wing blade clones from nonpermeabilized discs were used for the analysis. Fluorescence values were quantified with MetaMorph (Meta Imaging Series 6.1, Universal Imaging Corporation, PA). In brief, each Z series was thresholded to remove background. Fluorescence was measured over equivalent areas from mutant and wild-type tissue for individual z-sections starting from the apical-most portion of the epithelium and proceeding basally for 4–10 μm at 0.2 μm increments. Values for individual clones were then summed for each genotype and used to determine the ratio of fluorescence between mutant and wild-type cells. Care was taken to ensure that the regions analyzed did not encompass variations in the endogenous pattern of Notch expression. Pairwise comparisons were made between the mean ratio (mutant/wild-type) at 0 min to the mean ratio at the later time points (10, 30, or 60 min) by means of a t test analysis (MS Excel).

Quantitative PCR

Total RNA was extracted from wing imaginal discs with Trizol (Invitrogen). Glycogen (Ambion) was added as a carrier to facilitate precipitation. The RNA was DNase (Ambion) treated and first strand synthesis was performed with TaqMan Reverse Transcription Reagents (Invitrogen). 1% of the resulting product was used as a template in a quantitative PCR reaction as described in the Light Cycler Fast Start DNA Master SYBR Green I kit (Roche), except that reactions were scaled down to 10 μl. PCR was performed with the Light Cycler System (Roche). RP49 was used for normalization. Results of four independent experiments were averaged.

Supplemental Data

Supplemental Data include six figures and can be found with this article online at http://www.current-biology.com/cgi/content/full/16/7/702/DC1/.

Acknowledgments

We are grateful to C. Ferguson, M. Glotzer, S. Haase, D. Kiehart, I. Rebay, and members of the Fehon laboratory for comments and critical reading of the manuscript. We would also like to thank N. Wesolowska for technical help and the many colleagues who have provided antibodies and other reagents. S.M. was the recipient of a Young Investigator Award from the National Neurofibromatosis Foundation. This work was supported by grant NS034783 from the National Institutes of Health.

Received: August 30, 2005
Revised: January 31, 2006
Accepted: February 15, 2006
Published: April 3, 2006

References

1. Johnston, L.A., and Gallant, P. (2002). Control of growth and organ size in *Drosophila.* Bioessays *24*, 54–64.
2. Bretscher, A., Edwards, K., and Fehon, R.G. (2002). ERM proteins and merlin: integrators at the cell cortex. Nat. Rev. Mol. Cell Biol. *3*, 586–599.
3. LaJeunesse, D.R., McCartney, B.M., and Fehon, R.G. (1998). Structural analysis of *Drosophila Merlin* reveals functional domains important for growth control and subcellular localization. J. Cell Biol. *141*, 1589–1599.
4. LaJeunesse, D.R., McCartney, B.M., and Fehon, R.G. (2001). A systematic screen for dominant second-site modifiers of *Merlin/NF2* phenotypes reveals an interaction with *blistered/DSRF* and *scribbler.* Genetics *158*, 667–679.
5. McCartney, B.M., and Fehon, R.G. (1996). Distinct cellular and subcellular patterns of expression imply distinct functions for the *Drosophila* homologues of moesin and the neurofibromatosis 2 tumor suppressor, merlin. J. Cell Biol. *133*, 843–852.

6. Boedigheimer, M.J., Nguyen, K.P., and Bryant, P.J. (1997). Expanded functions in the apical cell domain to regulate the growth rate of imaginal discs. Dev. Genet. *20*, 103–110.
7. McCartney, B.M., Kulikauskas, R.M., LaJeunesse, D.R., and Fehon, R.G. (2000). The *Neurofibromatosis-2* homologue, *Merlin*, and the tumor suppressor *expanded* function together in *Drosophila* to regulate cell proliferation and differentiation. Development *127*, 1315–1324.
8. Lee, J.D., and Treisman, J.E. (2002). Regulators of the morphogenetic furrow. In Results and Problems in Cell Differentiation, Volume *37*, *Drosophila* Eye Development Edition, K. Moses, ed. (Berlin: Springer-Verlag), pp. 21–34.
9. Silver, S.J., and Rebay, I. (2005). Signaling circuitries in development: insights from the retinal determination gene network. Development *132*, 3–13.
10. Kumar, J.P., and Moses, K. (2001). The EGF receptor and notch signaling pathways control the initiation of the morphogenetic furrow during *Drosophila* eye development. Development *128*, 2689–2697.
11. Lee, J.D., and Treisman, J.E. (2001). The role of Wingless signaling in establishing the anteroposterior and dorsoventral axes of the eye disc. Development *128*, 1519–1529.
12. Chanut, F., and Heberlein, U. (1997). Role of *decapentaplegic* in initiation and progression of the morphogenetic furrow in the developing *Drosophila* retina. Development *124*, 559–567.
13. Dominguez, M., and Hafen, E. (1997). Hedgehog directly controls initiation and propagation of retinal differentiation in the *Drosophila* eye. Genes Dev. *11*, 3254–3264.
14. Sturtevant, M.A., O'Neill, J.W., and Bier, E. (1994). Down-regulation of *Drosophila* Egf-R mRNA levels following hyperactivated receptor signaling. Development *120*, 2593–2599.
15. Jennings, B., Preiss, A., Delidakis, C., and Bray, S. (1994). The Notch signalling pathway is required for Enhancer of split bHLH protein expression during neurogenesis in the *Drosophila* embryo. Development *120*, 3537–3548.
16. Le Borgne, R., Bardin, A., and Schweisguth, F. (2005). The roles of receptor and ligand endocytosis in regulating Notch signaling. Development *132*, 1751–1762.
17. Zecca, M., Basler, K., and Struhl, G. (1996). Direct and long-range action of a wingless morphogen gradient. Cell *87*, 833–844.
18. Rebay, I., Fortini, M., and Artavanis-Tsakonas, S. (1993). Analysis of phenotypic abnormalities and cell fate changes caused by dominant activated and dominant negative forms of the Notch receptor in *Drosophila* development. C. R. Acad. Sci. III *316*, 1111–1123.
19. Cadigan, K.M., Jou, A.D., and Nusse, R. (2002). Wingless blocks bristle formation and morphogenetic furrow progression in the eye through repression of Daughterless. Development *129*, 3393–3402.
20. Le Roy, C., and Wrana, J.L. (2005). Clathrin- and non-clathrin-mediated endocytic regulation of cell signalling. Nat. Rev. Mol. Cell Biol. *6*, 112–126.
21. Cao, T.T., Deacon, H.W., Reczek, D., Bretscher, A., and von Zastrow, M. (1999). A kinase-regulated PDZ-domain interaction controls endocytic sorting of the beta2-adrenergic receptor. Nature *401*, 286–290.
22. Hamaratoglu, F., Willecke, M., Kango-Singh, M., Nolo, R., Hyun, E., Tao, C., Jafar-Nejad, H., and Halder, G. (2006). The tumour-suppressor genes *NF2*/*Merlin* and *Expanded* act through *Hippo* signalling to regulate cell proliferation and apoptosis. Nat. Cell Biol. *8*, 27–36.
23. Fehon, R.G., Johansen, K., Rebay, I., and Artavanis-Tsakonas, S. (1991). Complex cellular and subcellular regulation of Notch expression during embryonic and imaginal development of *Drosophila*: implications for Notch function. J. Cell Biol. *113*, 657–669.
24. Tomlinson, A., Bowtell, D.L., Hafen, E., and Rubin, G.M. (1987). Localization of the sevenless protein, a putative receptor for positional information in the eye imaginal disc of *Drosophila*. Cell *51*, 143–150.
25. Asano, M., Nevins, J.R., and Wharton, R.P. (1996). Ectopic E2F expression induces S phase and apoptosis in *Drosophila* imaginal discs. Genes Dev. *10*, 1422–1432.
26. Fehon, R.G., Dawson, I.A., and Artavanis-Tsakonas, S. (1994). A *Drosophila* homologue of membrane-skeleton protein 4.1 is associated with septate junctions and is encoded by the *coracle* gene. Development *120*, 545–557.
27. Fehon, R.G., Kooh, P.J., Rebay, I., Regan, C.L., Xu, T., Muskavitch, M.A.T., and Artavanis-Tsakonas, S. (1990). Molecular interactions between the protein products of the neurogenic loci *Notch* and *Delta*, two EGF-homologous genes in *Drosophila.* Cell *61*, 523–534.